Journal of Marine Research, 61, 411–434, 2003

Journal of
MARINE RESEARCH

Volume 61, Number 4

The role of outflow geometry in the formation of the recirculating bulge region in coastal buoyant outflows

by Greg Avicola[1,2] and Pablo Huq[1]

ABSTRACT

Density-driven coastal currents are a common feature in the world's coastal oceans. These currents may separate from the coastline due to variations in geometry. Past studies have shown that this separation may produce two distinctly different flow states: a continuation of the coastal current, or a recirculating gyre downshelf of, and attached to, the separation point. Laboratory experiments of coastal buoyant outflows (rotationally dominated, buoyancy driven) were undertaken to examine the role of bay geometry on the evolution of the outflow. Experiments were conducted on a rotating turntable in relatively deep water (such that the buoyant layer depth was much less than the total ocean depth). The geometry of the bay-exit was varied, both in exit angle (θ) and in radius of curvature (r_c). The width of the bay was varied such that the bay exit Kelvin number (a ratio between the width of the bay exit and the internal Rossby deformation radius) was order 1 for all experiments. A recirculating bulge (a large, anticyclonic gyre joining the coastal current to the buoyant source) was occasionally observed to form. Results are compared to the Bormans and Garrett (1989) hypothesis: this hypothesis is found to explain a portion of the results only. Geometrical arguments are presented that build upon the Bormans and Garrett hypothesis that parameterizes the magnitude of the flow separation between the buoyant fluid and the exit. A separation ratio, Γ, is defined as a ratio between the inertial turning radius of the flow and the maximum offshore distance between the separated flow and the coast. A recirculating bulge was observed to form for flows with values of $\Gamma > 0.5$. The separation ratio, Γ, is shown to be equivalent to the impact angle, Φ, of the buoyant fluid re-encountering the wall. The impact angle governs the upshelf and downshelf volume flux of the impacting fluid: recirculating bulge formation is found to occur when at least 50% of the source volume flux returns to the source region. This is equivalent to an impact angle greater than or equal to 60-degrees.

1. College of Marine Studies, University of Delaware, Newark, Delaware, 19716, U.S.A. ***email: huq@udel.edu***
2. Present address: College of Oceanic and Atmospheric Sciences, Oregon State University, Corvallis, Oregon, 97331, U.S.A.

1. Introduction

Localized sources of buoyant water are common in the coastal ocean: the buoyant plumes formed from such sources may possess a number of different flow structures, depending on the local conditions. The specific form of a particular buoyant outflow can be influenced by ambient currents, winds, tides, the geometry of the coastline, and bottom topography. This study examines the role of exit geometry upon the development of coastal currents utilizing laboratory simulations.

The motivation for examining the effect of variations of the exit geometry upon coastal current development is based upon oceanic observations. Observational studies of buoyant outflows have found that, in many cases, a coastal current forms directly outside the mouth of the source, continuing downshelf for a distance of $O(100)$ Rossby radii. Such studies include observations of the Delaware Coastal Current (e.g. Münchow and Garvine, 1993a,b), and the Hudson River Plume (e.g., Bowman and Iverson, 1978). However, in some cases a recirculating anticyclonic bulge (or gyre) has been observed to form directly downshelf and offshore of the source region, in addition to the usual coastal current. This gyre is large (in across-shelf extent) compared to the associated coastal current and acts as an intermediate flow structure between the buoyant source and the downshelf flow. Examples of such systems include observations of the Tsugaru warm current (e.g., Kawasaki and Sugimoto, 1984) and the Alboran Current (e.g., Lanoix, 1974). Figure 1 is composed of two images of large-scale buoyant outflows. The images are reproductions of the Alboran Gyre-Coastal Current system (image taken from Bormans and Garrett, 1989) and the Greenland freshwater jet (image taken from Bacon *et al.,* 2002). These images demonstrate the problem of interest: both images show large-scale buoyancy driven currents which are turned through relatively large angles. In the upper panel, the Alboran Gyre forms, while in the lower panel, the Greenland jet stays attached to the coastline.

Past numerical and laboratory studies have examined this phenomenon. Bormans and Garrett (1989) conducted laboratory simulations that examined the role of the radius of curvature of the coastal wall in regards to the formation of the recirculating bulge. Chao and Boicourt (1986) examined a model configuration with an estuary set perpendicular to the coastline exiting into a deep basin. Their results show a formation of a coastal current moving downshelf (in the direction of Kelvin-wave propagation), with a large recirculating region near the mouth. Subsequent simulations by Oey and Mellor (1993) conducted with higher resolution clearly show the formation of a large bulge region. Nof and Pichevin (2001) have suggested dynamical arguments for the formation and growth of such features, based upon momentum conservation.

This study attempts to explain the role of the bay-exit geometry in the formation of the recirculating bulge. The bay-exit geometry used in these experiments has been simplified such that it can be characterized by two parameters. The first parameter is the exit angle, θ, which characterizes the orientation of the axis of the estuary with respect to the axis of the coastline. An exit angle of 90-degrees denotes an estuary with a channel axis perpendicular to the coastline. Conversely, an exit angle of 0-degrees denotes an outflow released parallel

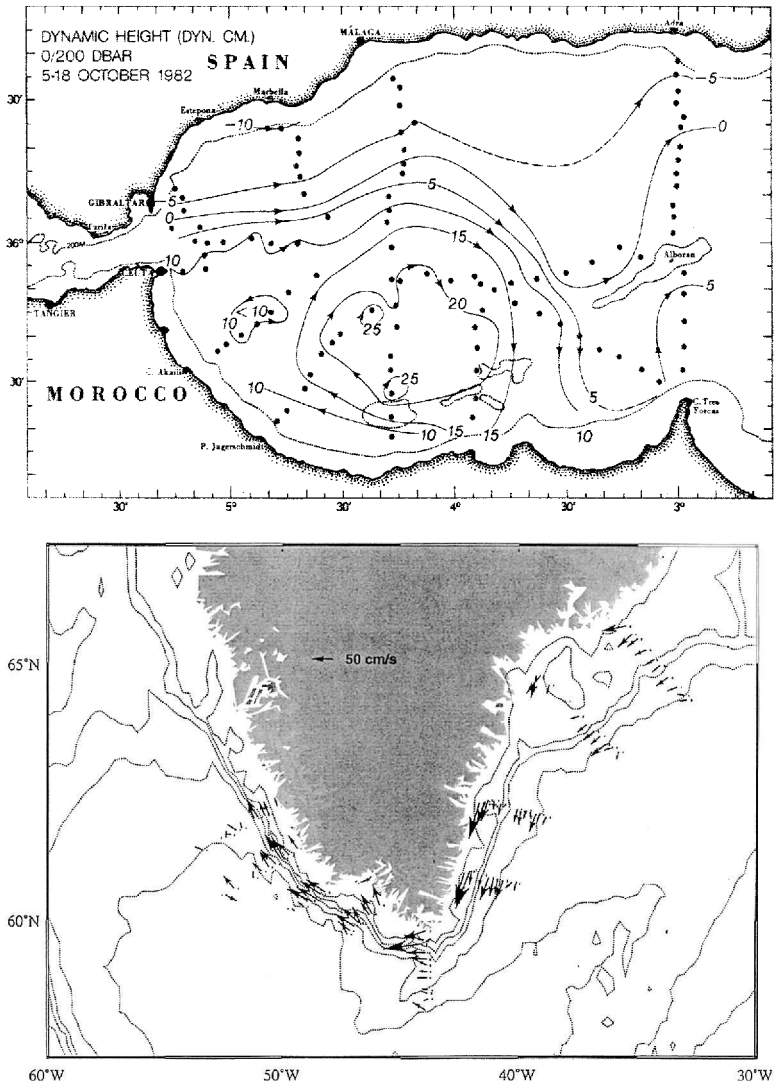

Figure 1. Reproductions of two large-scale buoyancy driven systems. The upper panel is a dynamic height map of the Alboran Gyre and coastal current system (reproduction from Bormans and Garrett, 1989—original data from Donde Va Group, 1984). Buoyant Atlantic water enters the Mediterranean through the Strait of Gibraltar. As seen in this dynamic height image, the system may form a gyre-coastal current system. The lower panel is an image of average surface currents taken from drifter data of the Greenland freshwater jet (reproduction from Bacon *et al.,* 2002).

to the coastline. The second parameter is the radius of curvature of the coastline, r_c. This parameter characterizes the 'sharpness' of the corner which joins the estuary coastline to the coastline of the ocean. A small value of the radius of curvature is indicative of a sharp transition (or corner) between the bay and the coastal ocean.

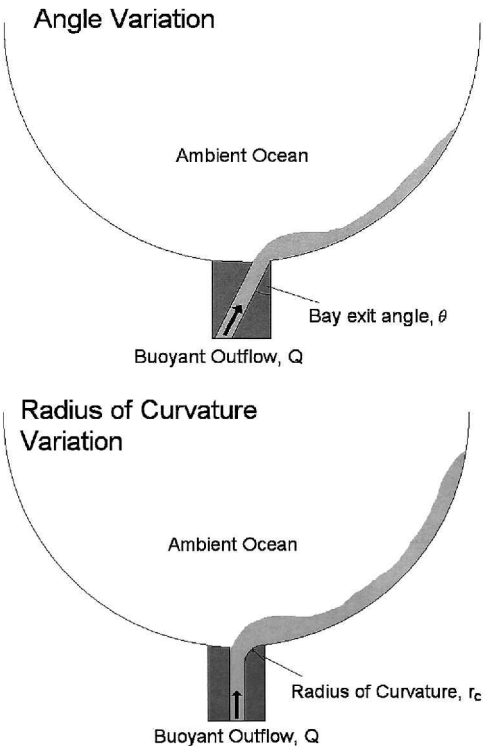

Figure 2. Schematic of the experimental setup for the experiments used in this study. Experiments were conducted on a turntable of 120 cm diameter. The turntable has a configurable 'shoebox' bay set along its circumference. Plexiglas inserts are available which may be inset into the bay in order to alter the dimensions of the bay exit (width, exit angle, radius of curvature). For the experiments presented in this study, the exit angle, θ, and radius of curvature, r_c, were varied, while the bay width was set to a constant outflow Kelvin number of one. The top panel portrays an experiment with a non-90-degree exit angle, while the lower panel portrays an experiment with a nonzero radius of curvature.

Schematics of the bay-exit geometrical variations are shown in Figure 2. The upper panel is a diagram depicting a buoyant outflow exiting an estuary with an arbitrary exit angle, θ, with a sharp radius of curvature ($r_c = 0$). The lower panel is a diagram depicting a buoyant outflow exiting a perpendicular bay ($\theta = 90°$) with an arbitrary radius of curvature, r_c. Both parameters may vary independently, in order to describe any particular estuary.

As this study is concerned with examining the impact of the bay geometry on the outflow, other relevant parameters were held constant. Experiments were conducted with a relatively thin buoyant outflow: that is, the buoyant outflow depth was small compared to the total ocean depth. Thus, the buoyant outflow was isolated from the bottom by a deep layer of relatively quiescent fluid: these experiments are classified as being surface

advected (Yankvosky and Chapman, 1997; Avicola and Huq, 2002). Additionally, all experiments were conducted such that the bay exit width was approximately equal to the internal Rossby radius of the outflow: this corresponds to a bay exit Kelvin number of order one.

As the recirculating bulge can be a relatively large feature in the coastal ocean, a better understanding of the dynamics behind the formation of the bulge is important. Often such bulges are formed from buoyant fluid originating from an estuary, and may contain pollution or biological material emanating from the (riverine) source with subsequent transport relatively far onto the continental shelf. Studies have established that the recirculating bulge grows with time and absorbs buoyancy flux that would otherwise be transported downshelf in the coastal current. Understanding the dynamics within the buoyant outflows in the coastal ocean is thus important. Additionally, the development or lack of development of such a flow structure may be an important consideration in understanding the life cycles of coastal organisms.

2. Experimental setup

Experiments were conducted in the Environmental Fluids Laboratory located within the College of Marine Studies, University of Delaware. The diameter of the turntable used in the experiments is 1.2 m. The turntable supported a tank. The tank is composed of a cylinder (with a flat bottom) and an attached bay. The bottom of the bay is flush with the bottom of the tank. The bay is constructed in such a manner that inserts can be placed within it to alter the plan geometry.

For the experiments, the outlet angle or the radius of curvature of the bay were varied through the use of such inserts. Five values for the exit angle were examined in these experiments ($\theta = 90°$, 75°, 60°, 45°, and 0°), with a radius of curvature $r_c = 0.1$ cm. Three values of the exit radius of curvature were examined ($r_c = 0.1$, 1.4, and 7.5 cm), with an exit angle $\theta = 90°$. Figure 2 is a schematic illustrating the experimental setup in plan view. All experiments were conducted for an estuary Kelvin number (defined as the ratio of the estuary width to the internal Rossby radius of the flow) of order one. Additionally, the ambient ocean depth (~10 cm) was an order of magnitude greater than the scale depth of the buoyant layer (~2 cm), resulting in a surface advected outflow (Yankovsky and Chapman, 1997; Avicola and Huq, 2002).

The cylindrical tank contained ambient ocean water of a specified salinity. A smaller reservoir filled with freshwater served as the source for the buoyant outflow. The source for these experiments was a pipe with a radius of 1 cm which was located at the head of the bay. The ambient ocean fluid was spun to solid body rotation before an experiment was begun. The turntable was rotated counterclockwise, resulting in a positive planetary vorticity, f. Leveling of the turntable removed measurable (artificial) tidal motions. The free-surface parabola induced from the rotation of the fluid is not dynamically significant: the topographic beta effect produced from this effect is two orders of magnitude smaller

Table 1. Table in which the physical parameters for the experiments conducted in this study are listed. Experiments in which a recirculating bulge were observed to form are shaded light gray. Tabulated, from left to right, are: Density anomaly, $\Delta\rho$; Coriolis parameter, f; Source volume flux, Q; Rossby radius, R; scale depth, h; inertial radius, u/f; bay exit angle, θ; bay radius of curvature, r_c; and the bay exit Rossby number (of Bormans and Garrett, 1989) uf/r_c. Experiments were conducted with two sets of source initial conditions (A-designated experiments—$\Delta\rho \sim 5, f \sim 1.2, Q \sim 10$; and B-designated experiments—$\Delta\rho \sim 15, f \sim 0.9, Q \sim 10$), along with variations in bay exit angle and bay radius of curvature. The bay exit Rossby number (uf/r_c) follows the trend shown in Bormans and Garrett (1989), Klinger (1994a,b), and Jiang (1985) for experiments in which radius of curvature was varied and exit angle was set at 90-degrees (the last 6 experiments listed). For those experiments, values of the bay exit Rossby number larger than one ($u/fr_c > 1$) were found in experiments in which a recirculating bulge did form. However, the bay exit Rossby number does not predict bulge formation for experiments in which the bay exit angle is varied.

Name	$\Delta\rho$	f	Q	R	h	u/f	θ	r_c	u/fr_c	BULGE?
units	kg/m^3	s^{-1}	cm^3/s	cm	cm	cm	deg	cm	—	—
A-Ang-90	5	1.3	10.0	2.6	2.3	1.3	90	0.1	13.2	YES
A-Ang-75	5.5	1.1	10.0	2.9	2.1	1.5	75	0.1	14.6	YES
A-Ang-60	5.5	1.3	10.0	2.7	2.2	1.4	60	0.1	13.6	No
A-Ang-45	5	1.3	10.0	2.6	2.3	1.3	45	0.1	13.2	No
A-Ang-0	5.25	1.3	10.0	2.7	2.2	1.3	0	0.1	13.4	No
B-Ang-90	14.5	0.9	9.5	4.4	1.1	3.3	90	0.1	33.2	YES
B-Ang-60	14	0.9	10.0	4.4	1.1	3.3	60	0.1	33.3	No
B-Ang-45	15	0.9	10.0	4.5	1.1	3.4	45	0.1	33.9	No
B-Ang-0	14.5	0.9	10.0	4.5	1.1	3.4	0	0.1	33.6	No
A-Rad-01	5	1.3	10.0	2.6	2.3	1.3	90	0.1	13.2	YES
A-Rad-14	6	1.3	10.8	2.8	2.2	1.4	90	1.4	1.0	No
A-Rad-75	5.5	1.3	10.0	2.7	2.2	1.4	90	7.5	0.2	No
B-Rad-01	14.5	0.9	9.5	4.4	1.1	3.3	90	0.1	33.2	YES
B-Rad-14	16	0.9	10.0	4.6	1.1	3.4	90	1.4	2.5	YES
B-Rad-75	15	0.9	10.0	4.5	1.1	3.4	90	7.5	0.5	No

than the primary forcing. Evaporative cooling and surface wind-stress were removed by the use of a Plexiglas cover.

Velocity data were collected with a Sony 450x digital video camcorder. The camcorder was suspended above and co-rotated with the tank. The buoyant outflow fluid was marked using Rhodomine dye, and the surface of the flow was seeded with reflective surface drifters, typically 0.5 mm in size. The dye served as a visual marker of the extent of the flowfield, while the drifters were tracked in space and time from the video records to provide information on recirculating bulge/coastal current dimensions and velocities.

Experimental results taken from thirteen parameter configurations are presented. Table 1 lists these experimental configurations. Runs are designated in the following format: *[X]-[Type]-[Value].* 'X' describes the geostrophic forcing of the experiment. Based on the source values of density anomaly, $\Delta\rho$, volume flux, Q, and Coriolis parameter, f,

geostrophic scales can be derived which nondimensionalize the coastal current. Data will be presented from two sets of source values: A-type experiments ($\Delta\rho \sim 5.5$ kg/m^3, $Q \sim 10$ m^3/s, $f \sim 1.26$ s^{-1}) and B-type experiments ($\Delta\rho \sim 15.0$ kg/m^3, $Q \sim 10$ m^3/s, $f \sim 0.89$ s^{-1}). 'Type' classifies which of the two exit parameters is varied: Ang-type experiments examine variations in exit angle, θ, with fixed radius of curvature, $r_c \sim 0.1$ cm; Rad-type experiments examine variations in radius of curvature, r_c, with a fixed angle, $\theta = 90°$. Finally, 'Value' refers to the value of the variation being considered. Thus, the experiment listed as *A-Ang-60* is an A-type experiment with a 60-degree outflow exit angle. Of the experiments listed in Table 1, two are duplicates. Experimental configuration *A-Ang-90* is identical to *A-Rad-01*. Similarly, experimental configuration *B-Ang-90* is identical to *B-Rad-01*. They are listed under two names to allow for easier comparison.

The experiments conducted in this study can be characterized by three variables that affect the scales of the buoyant outflow, independent of the particular characteristics of the bay exit. These three variables are listed in the first three columns of Table 1: the reduced gravity of the source, g'_0, the Coriolis parameter of the system, f, and the volume flux of the source, Q_0. From these values, dynamically relevant scales of the buoyant plume can be derived.

These buoyant plume scales are formed from the dynamics of a two-layer density-driven front in thermal wind balance. The volume transport within such a frontal structure is simply:

$$Q_g = \frac{z^2 g'}{2f} \tag{1}$$

where Q_g represents the volume transport in the front. The variable z represents the maximum depth of the front, and g' is the local reduced gravity associated with the front. A scale-depth, h, can be derived from Eq. 1 by setting the volume transport of the front, Q_g, equal to the source volume flux, Q_0, and setting the local reduced gravity, g', equal to the reduced gravity of the source, g'_0.

$$h = \sqrt{\frac{2Q_0 f}{g'_0}}. \tag{2}$$

This scale depth, h, will be used to nondimensionalize the vertical measurements of the buoyant outflow. From this scale depth, h, the horizontal length scale, R, is obtained. This horizontal length scale, R, is the internal Rossby radius of the buoyant outflow, and will be used to nondimensionalize the horizontal measurements of the buoyant outflow.

$$R = \frac{\sqrt{g'_0 h}}{f}. \tag{3}$$

Similarly, the internal wave speed, c, will be used to nondimensionalize velocity measurements, where c is written:

$$c = \sqrt{g_0' h}. \tag{4}$$

Finally, temporal measurements will be nondimensionalized by the rotation period of the system, T.

3. Formation of a recirculating bulge

The focus of this study is to establish when a buoyant outflow will produce a recirculating bulge, and the consequence of the recirculating bulge formation on a downstream coastal current. Visually, it is obvious when an experiment has formed a recirculating bulge, which can be described as an approximately circular feature located just downshelf and offshore of the bay mouth. This feature is observed to grow with time, rotate with negative (clockwise) vorticity, and is large in size compared to the coastal current scale, R.

Table 1 lists the characteristics of experiments that were observed to form recirculating bulges, and those which did not. For ease of reference in the table, experiments in which recirculating bulge formation occurred have been shaded with a light gray background. A bulge formed in four of the thirteen experiments (*A-Ang-90/A-Rad-01, B-Ang-90/B-Rad-01, A-Ang-75* and *B-Rad-14*).

Figure 3 comprises three schematics: the schematics illustrate the initial stages of recirculating bulge formation for a $K = 1$ outflow, with a bay exit angle, $\theta = 90°$, and a radius of curvature, $r_c = 0$ cm. The schematics of Figure 3 are representative illustrations of the observed evolution during the initial stages of a buoyant outflow. Initially, the buoyant outflow exits the bay: the primary velocity component of the buoyant fluid points in the offshore direction. This is illustrated in the upper panel of Figure 3. However, the buoyant fluid responds to the Coriolis force of the rotating system by accelerating to its right, thereby turning in an inertial circle. The buoyant fluid turns approximately 180 degrees, at which point it impacts the wall. The impact occurs at a time roughly ¼ of a rotation period (¼ T) from the point in time that it exited the bay mouth. This time of impact is depicted in the middle panel. Continuity requires that the impacting fluid must flow either upshelf or downshelf: in fact, it is observed to do both. The downshelf portion of the buoyant fluid forms the coastal current. The upshelf portion of the buoyant fluid returns to the vicinity of the bay mouth, where it is re-entrained into the exiting fluid. This recirculation continues and becomes the recirculating bulge. This stage of evolution is depicted in the lower panel of Figure 3.

A number of observations can be made based upon this description of recirculating bulge formation. Firstly, it is clear that the buoyant fluid must separate from the coastal wall in order to form the recirculating bulge. Secondly, the impact of the stream of the buoyant fluid with the coastal wall, during its reattachment, plays a role in the development of the bulge. Clearly, it is the impact that partitions the stream of buoyant fluid into two streams; an upshelf return flow, which forms the recirculating bulge: and a downshelf flow, which forms the coastal current.

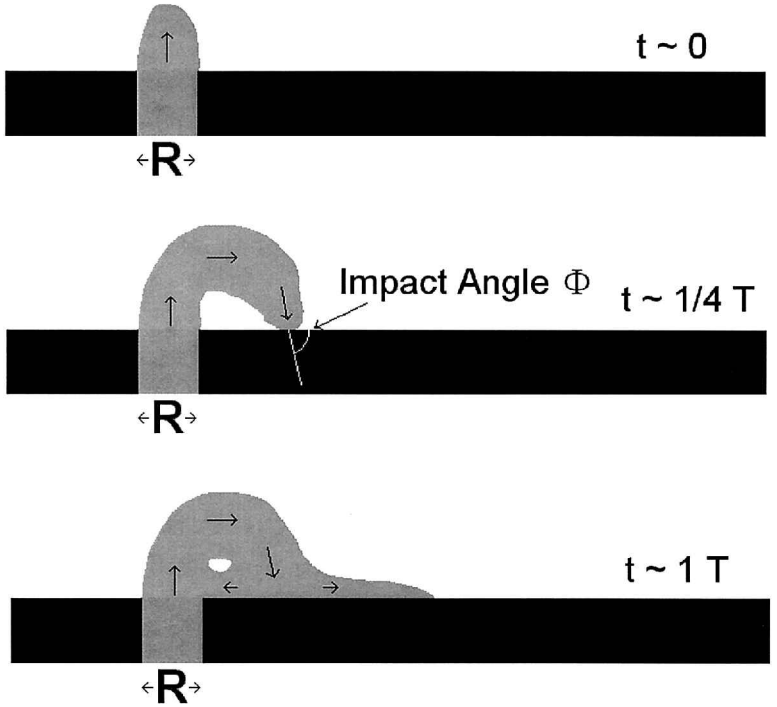

Figure 3. Schematic which portrays the initial stages of a buoyant outflow exiting a Kelvin number ($K = W/R = 1$) Estuary set at 90-degrees to the coastline with a sharp radius of curvature. Such an outflow forms a recirculating bulge in the manner shown. The upper panel shows the buoyant outflow shortly after it exits the bay. As time evolves, the buoyant outflow is deflected by the Coriolis force and makes half of an inertial circle, at which point it impacts the wall. This is shown in the middle panel, and occurs at a time of approximately ¼ of a rotation period. The buoyant outflow impacting the wall diverges into an upshelf and a downshelf flow. In this situation, the upshelf (return) flow is large, and a recirculating bulge forms as is shown in the lowest panel.

a. The effect of radius of curvature

Some aspects of the formation mechanism of a recirculating bulge have been examined previously: Bormans and Garrett (1989) utilized laboratory experiments to examine whether or not an outflow would produce a 'gyre' (recirculating bulge) or 'jet' (coastal current only). Their experiments were conducted via a dam-break configuration; a turntable was divided into two basins by a wall. The two basins were joined via a single strait, through which an exchange flow produced a buoyant current. They predicted experiments would fall into either a 'jet' or a 'gyre' mode based upon a simple criterion: that a recirculating bulge would form if $u/f > r_c$ (where u is the velocity of the fluid turning the corner). The experiments confirmed this hypothesis.

The hypothesis is based upon a ratio of length scales. The radius of curvature length-scale, r_c, is simply the radius of the corner. The other relevant length scale is the

radius of the inertial turn, u/f: the value u/f corresponds to the radius of the inertial circle taken by a parcel of fluid moving at velocity u, in a rotating frame of reference. Thus, the criterion simply compares the radius of curvature of the corner to the radius of curvature of the fluid parcel's inertial turn. If the radius of curvature of the corner is smaller than the radius of the inertial turn, the fluid will separate from the wall. The criterion of Bormans and Garrett can be rewritten as a bay exit Rossby number, $Ro = u/fr_c$. For values of the bay exit Rossby number greater than one ($Ro = u/fr_c > 1$) a recirculating bulge is expected to form.

This result was examined analytically in two studies: Klinger (1994a) and Jiang (1995). Their analysis was based upon a density front (coastal current) attached to a vertical wall. The fluid is assumed Boussinesq, hydrostatic, and inviscid. Furthermore, the values of derivatives of across-shore properties (temperature, density, velocity) are typically orders of magnitude larger than the along-shore derivatives in such a front. Thus, the along-shore derivatives are neglected. Finally, the coastal current is assumed to be in steady state. Based upon these approximations, Klinger (1994a) and Jiang (1995) began with the across-shore momentum and potential vorticity equations. This requires one to solve for the critical value for the radius of curvature, defined as the radius of curvature for which the buoyant layer touches the surface at the coastal wall. Both authors found, to a very good approximation, that the flow will separate from the wall if $0.9\ u/f > r_c$, or stated in terms of the exit Rossby number, that $Ro = u/fr_c > 1.1$. The value of the potential vorticity, δ, of the coastal current was varied, but was found to have negligible impact on this result.

The experiments conducted in this study are compared to the Bormans and Garrett criterion of u/fr_c. In order to make such a comparison, the velocity of the coastal current must be known as the current rounds the corner. The experiments conducted for this study were done with a bay-exit Kelvin number of order one. The resulting velocity exiting the source must therefore have a Froude number of order one as well. Velocity measurements were made for each experiment directly outside of the source region to ascertain the actual velocity of the buoyant outflow as it exited the bay. It was found that the current turned the corner at an exit of approximately 0.5 c for "A" experiments and 0.75 c for "B" experiments. These velocities translate to values of $u/f \sim 0.5\ R$ and $0.75\ R$ respectively, for the radius of the inertial turn.

The last six experiments listed in Table 1 were experiments with a constant exit angle, $\theta = 90°$, and variable radius of curvature, r_c. Thus, these experiments examine the role of the bay-exit geometry in the same manner as the experiments of Bormans and Garrett. Experiments *A-Rad-01, B-Rad-01,* and *B-Rad-14* formed recirculating bulge regions; for these experiments the values of the bay exit Rossby number, $Ro = u/fr_c$, were 13.3, 33.2 and 2.5, respectively. Experiments *A-Rad-14, A-Rad-75* and *B-Rad-75* did not form a recirculating bulge; with values of the bay exit Rossby number of 1.0, 0.2 and 0.5, respectively. These results have been portrayed graphically in Figure 4: the ordinate is the Froude number of the flow rounding the corner, while the abscissa is a ratio of the Rossby radius to the radius of curvature (R/r_c). The product of the abscissa and the ordinate is the

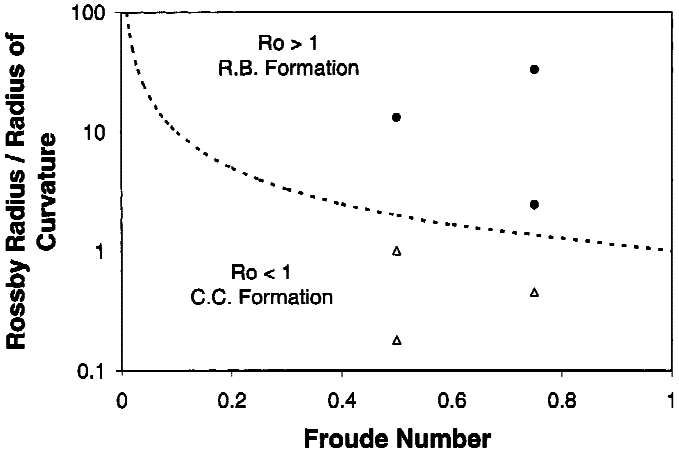

Figure 4. Graph of experimental data from this study plotted in the manner of Bormans and Garrett (1989). Data have been plotted for the experiments in which the exit outflow was 90-degrees, but the radius of curvature was varied. The open triangles indicate experiments in which no recirculating bulge formed, while the solid circles indicate experiments in which one did. The ordinate comprises values of R/r_c, while the abscissa comprises values of $Fr = u/c$. Values of the bay exit Rossby number equal to one, $Ro = u/fr_c = 1$, are shown as the dashed line. Experiments with a recirculating bulge formation all lie above the dashed line of the hypothesis of Bormans and Garrett (1989).

outflow Rossby number, $Ro = u/fr_c$. Values of the Rossby number, $Ro = 1$, are shown as the dashed line. Larger values of the Rossby number, $Ro > 1$, lie above this line, while smaller values of the Rossby number, $Ro < 1$, lie below. Experiments in which a recirculating bulge formed are marked with a circle, while those in which no bulge formed are marked with a triangle. Experiments in which a recirculating bulge formed all lie above the line in Figure 4, in accord with the hypothesis of Bormans and Garrett (1989).

b. Exit angle and its impact on recirculating bulge formation

In the experiments conducted by Bormans and Garrett, runs were all conducted with a 90° exit angle. To examine the role of the exit angle, the upper nine experiments in this study (Table 1) were conducted with exit angles varying between 0° and 90°. This allows for the discrimination of the role of exit angle on the formation of the recirculating bulge. For those nine experiments, the exit angle, θ, was varied, but the exit radius of curvature was small, $r_c = 0.1$ cm. The type-"A" experiments possess values of the Rossby number $Ro = u/fr_c$ of approximately 13.5; while the type-"B" experiments possess values of the Rossby number of approximately 33.5. Clearly, all nine experiments have values of the bay exit Rossby number large enough to produce separation ($u/fr_c > 1$ in all nine experiments). Yet, in all but three cases (*A-Ang-90, A-Ang-75,* and *B-Ang-90*), no recirculating bulge is seen to form.

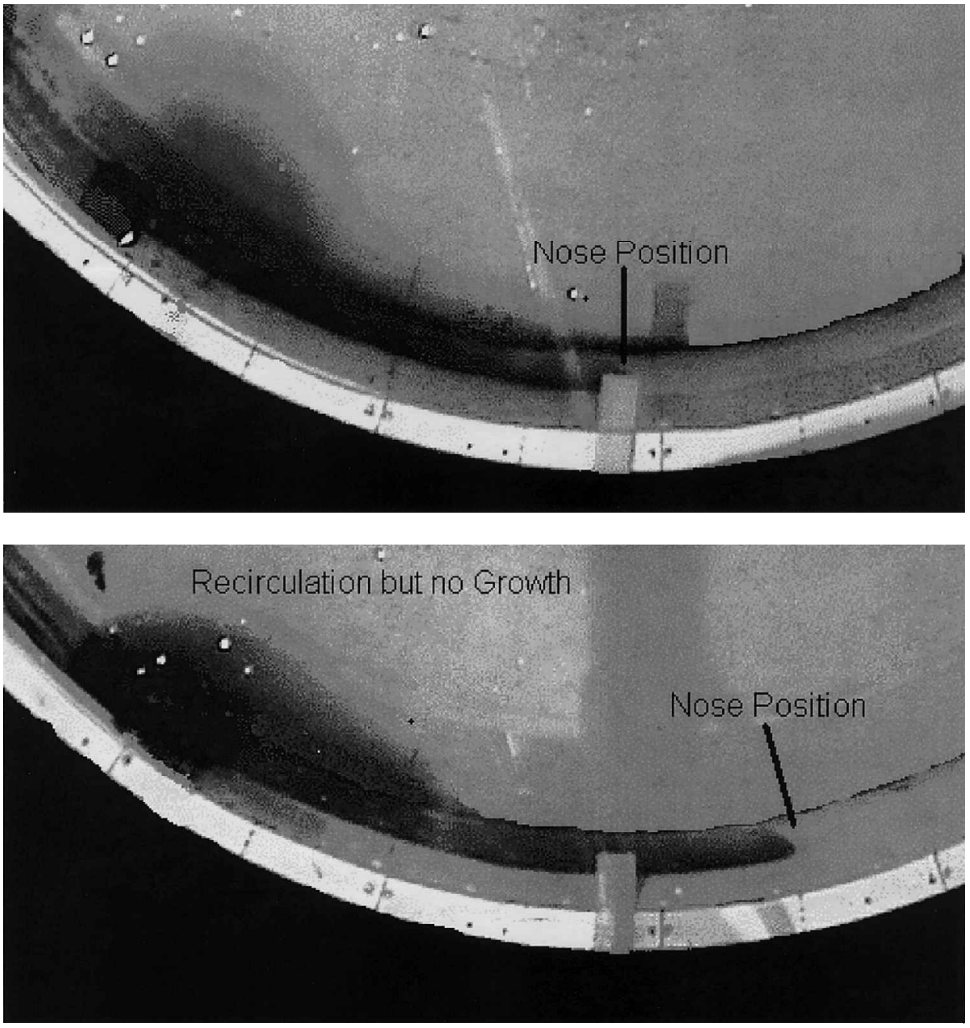

Figure 5. Images of four experiments digitized from video records. The four experiments have identical experimental parameters ("B" type experiments) save for the exit angle. The exit angle for each panels A, B, C and D, are 90°, 60°, 45° and 0°, respectively. These images were taken one rotation period after the buoyant outflow exited the estuary. Note that only the Panel A experiment ($\theta = 90°$) was observed to form a recirculating bulge: the experiment shows a characteristic circular bulge and a significantly shorter coastal current than observed in the other three experiments.

The effect of exit angle on recirculating bulge formation can be seen visually in images of the experiments. Figure 5 shows four digital images taken from the digital video record of experiments *B-Ang-90, B-Ang-60, B-Ang-45* and *B-Ang-0.* The four experiments have identical experimental parameters ("B" type experiments) save for the exit angle. These

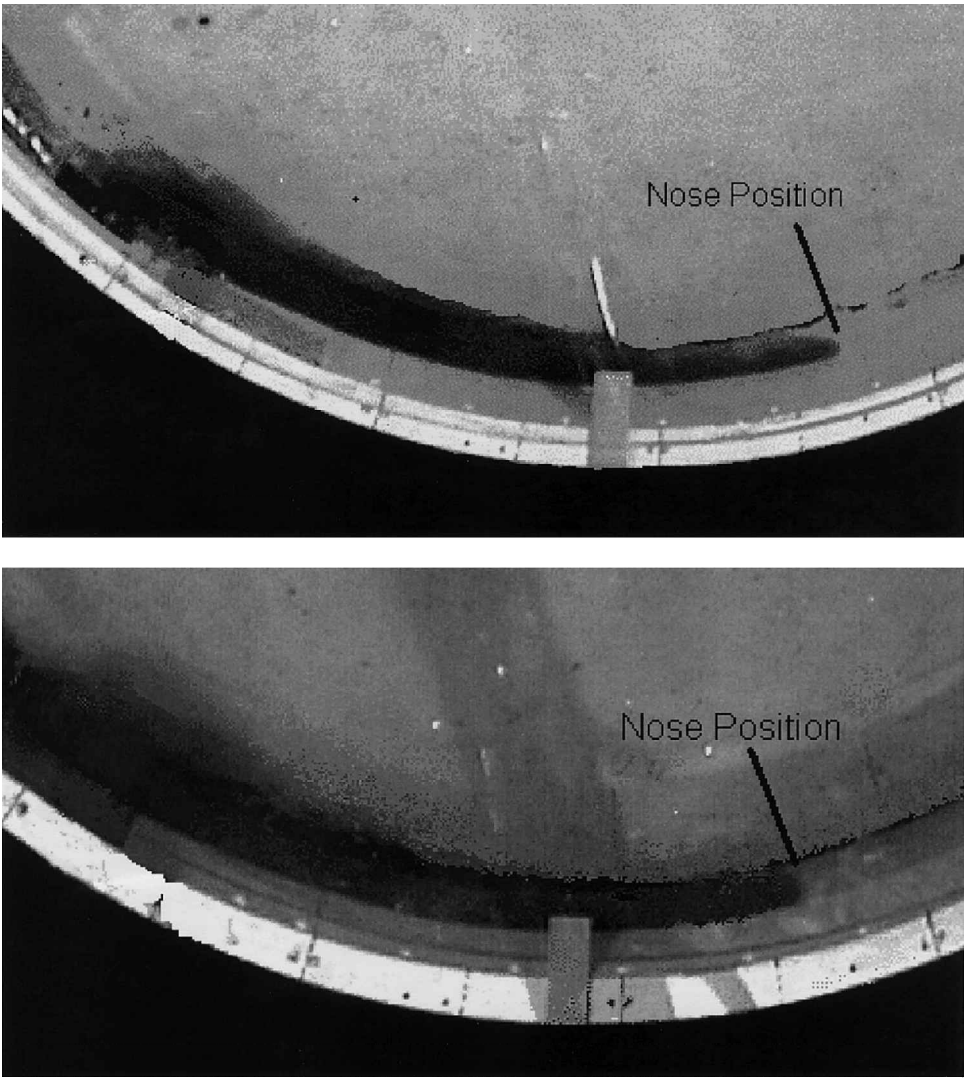

Figure 5. (Continued)

pictures were captured approximately 1 rotation period after the buoyant outflow exited the estuary. Note that only the left-most experiment ($\theta = 90°$) was observed to form a recirculating bulge: the experiment shows a characteristic circular bulge (which grows with time) and a significantly shorter coastal current than observed in the other three experiments. The middle two experiments ($\theta = 60°, 45°$) show a flow separation region, with some associated recirculation. However, this recirculation region does not grow with time, and the coastal current growth rate is identical between the two experiments and the

last experiment ($\theta = 0°$). This can be seen in the length of the coastal current of the four pictures after a time of one rotation period. This trend becomes increasingly obvious at later times.

Clearly, flow separation, as characterized by the ratio of curvature length scales, is an important aspect of recirculating bulge formation, but does not solely account for the process. A coastal current which flows past a very sharp corner will separate; however, if the corner has only a very slight angle, the deviation of the flow from the coastline will be very small. We propose that the 'significance' of the separation of a density-driven current can be examined via a ratio of length scales. The magnitude of the separation from the wall can be defined by a separation distance, d. The separation distance is a measure of the maximum offshore separation between the buoyant outflow and the coastal wall. A nondimensional separation ratio, $\Gamma = df/u$, is formed as the ratio of the magnitudes of the separation distance, d, and the inertial turn radius, u/f. Values of the separation ratio, Γ, may vary between zero and one. A value of zero occurs when the buoyant outflow does not separate from the wall; the separation distance, d, is zero, and the separation ratio is zero. A value of one is possible when the separation distance, d, is equal to the inertial turn radius, u/f. This is the maximum separation distance possible for the coastal geometries examined in this study.

Figure 6 contains four schematics that visually portray the concept of the separation distance, d, and the separation ratio, Γ. Panel A depicts the situation in which a buoyant outflow exits a bay with a small radius of curvature ($r_c \sim 0$ cm) at a 90-degree angle ($\theta = 90°$). Given that the radius of curvature is zero, the maximum separation distance is simply the radius of the inertial turn: $d = u/f$. This situation has a value for the separation ratio of, $\Gamma = 1$. It is also possible to define an impact angle, Φ, or the angle at which the buoyant outflow impacts the wall at its point of reattachment. A value of the impact angle, $\Phi = 90°$, indicates that the flow is impacting the wall such that the velocity vector of the buoyant fluid is perpendicular to the coastline.

A buoyant outflow exiting a bay with an arbitrary radius of curvature (r_c) at a 90-degree angle ($\theta = 90°$) is shown in Panel B. If $r_c > u/f$ the plume does not detach. If $r_c < u/f$, the plume detaches and the separation distance is simply $d = u/f - r_c$, which results in a separation ratio, $\Gamma = 1 - fr_c/u$. The impact angle will be ($\Phi = \cos^{-1}(1 - uf/d)$). Panel C represents the case in which the radius of curvature is zero ($r_c \sim 0$ cm) and the exit angle is between 0 and 90-degrees: also shown are the appropriate expressions for d, Γ, and Φ.

Finally, Panel D shows the general case of arbitrary radius of curvature and exit angle. For this situation, the turning radius of the plume and the exit configuration can be shown to produce the following values for d, Γ, and Φ:

$$d = \left(\frac{u}{f} - r_c\right)(1 - \sin(90 - \theta)) \tag{5}$$

$$\Gamma = \frac{df}{u} = \left(1 - \frac{r_c f}{u}\right) \sin(90 - \theta) \tag{6}$$

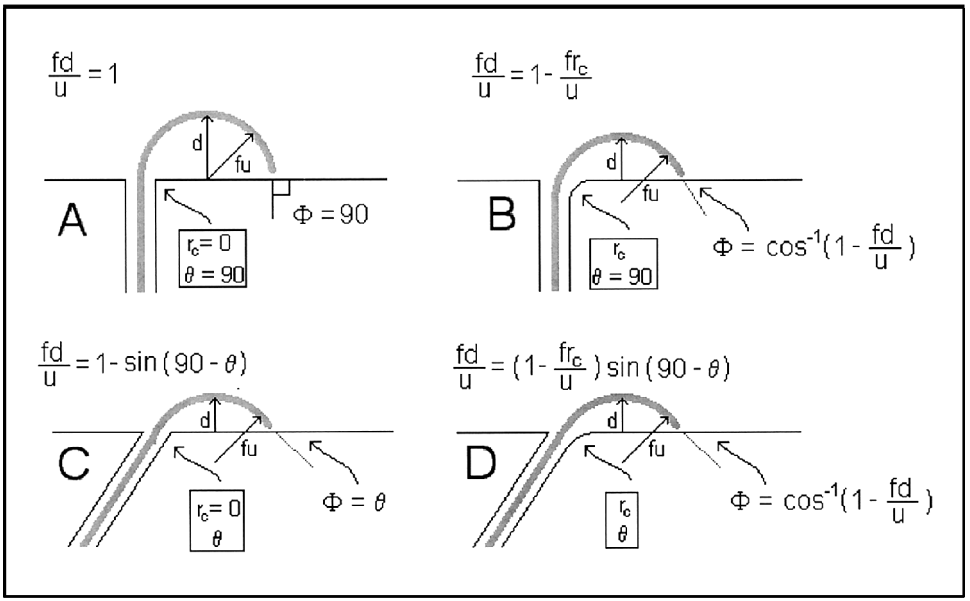

Figure 6. Diagram of the geometrical construct used to examine recirculating bulge formation. The radius of the inertial circle for a particular outflow is shown as the line u/f. The exit angle of the bay, θ, and the radius of curvature, r_c, are shown. These three variables determine the maximum separation distance of the centerline, d, the separation ratio, $\Gamma = fd/u$, and the impact angle, Φ, of the buoyant fluid. Panel A depicts the case with a 90-degree bay and a radius of curvature of zero, which is a typical configuration for many past numerical and laboratory studies. Panel B depicts a more generalized case, in which the exit angle is 90-degrees, but the radius of curvature is nonzero. Such a configuration was used in Bormans and Garrett (1989). Panel C depicts a situation in which there is a sharp corner, with a radius of curvature of zero, but an arbitrary non-90-degree exit angle. Finally, Panel D depicts the most general case, with an arbitrary nonzero exit angle and nonzero radius of curvature. The general expressions for the separation ratio, fd/u, and the impact angle, Φ, are shown.

$$\phi = \cos^{-1}\left(1 - \frac{df}{u}\right). \tag{7}$$

This integrates the effect of a radius of curvature, bay exit angle, and geostrophic flow characteristics into a separation ratio, Γ, or impact angle, Φ.

It is important to note that the quantities in Eqs. 5–7 and the flow described in Figure 6 are only relevant during the initial stages of evolution of the buoyant outflow. The dynamics described here are valid when the outflow first exits a bay or estuary, and makes an inertial turn to impact the coastal wall. However, note that these quantities will not be constant throughout the evolution of the buoyant plume: in fact, observations of recirculating bulge (examined in the companion paper, Avicola and Huq, 2003) indicate that the recirculating bulge grows in time. Therefore, the argument is made that it is the dynamics

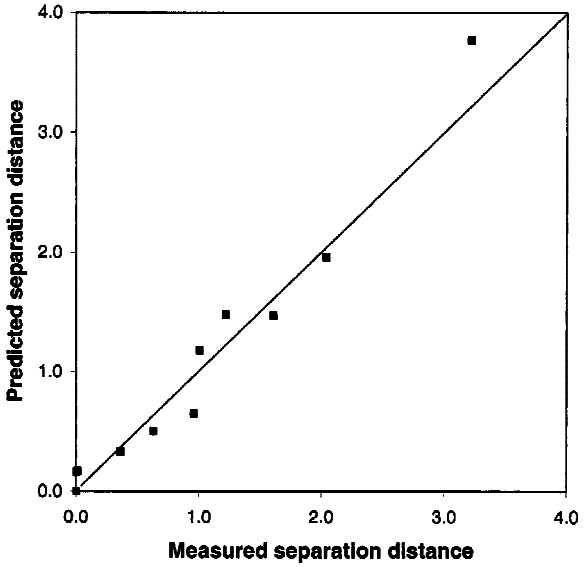

Figure 7. Graph in which the observed (abscissa) and the predicted (ordinate) separation distance are plotted for the experiments presented in this study. The solid line corresponds to an observed versus predicted ratio of one. Predicted values of the separation distance, d, are calculated (Eq. 5) based upon the inertial turning radius, u/f, the exit angle, θ, and the exit radius of curvature, r_c of the experiment. Measured values of the separation distance, d, are obtained from video records of the experiments. As the buoyant outflow exits the bay, it may separate from the wall. If it separates, at some subsequent point in time, it will impact the wall. The video record is examined at this time (the impact point) and a centerline of the buoyant plume is traced between the bay exit and the impact point. The measured separation distance, d, is defined as the maximum distance observed between the centerline of the plume and the coastline, minus the distance between the plume centerline and the coastline for the zero-degree exit angle case (which does not separate).

of the initial impact that determines the fate of the outflow: either a recirculating bulge will form or it will not.

Comparison between the predicted values of the separation distance and the direct observations from experiments was undertaken. For each experiment, the video record was observed as the buoyant outflow exited the bay, turned an inertial circle, and finally impacted the wall. At the point in time when the plume was observed to impact the wall, the separation distance, d, was measured. The measured value of the separation distance was defined as the maximum distance between the coastline and the centerline of the plume, minus the distance between the coastline and the centerline of the plume for a nonseparating case (0-degree exit angle). Plotted in Figure 7 is the predicted separation distance (Eq. 5) versus the observed separation distance. The solid line shown in Figure 7 represents the line on which the predicted separation distance equals the observed separation distance. The experimental data, plotted as solid squares, are in good agreement with this line, demonstrating the utility of the separation distance, d.

Table 2. Table in which the impact parameters for the experiments conducted in this study are listed. Experiments in which a recirculating bulge was observed to form are shaded in light gray. Tabulated, from left to right, are bay exit angle, θ; bay radius of curvature, r_c; bay Rossby number, u/fr_c; predicted separation distance, d; separation ratio, df/u; and predicted impact angle, Φ. The separation ratio, df/u, differentiates between experiments in which a recirculating bulge forms and those in which it does not, for variations in both radius of curvature and exit angle. For values of the separation ratio larger than 0.5 ($df/u > 0.5$) a recirculating bulge is seen to form. The separation ratio can be used to calculate an impact angle, Φ. For impact angles larger than 60 degrees ($\Phi > 60$) a recirculating bulge is observed to form.

Name	BULGE?	θ	r_c	u/fr_c	Predicted d	df/u	Predicted ϕ
units	—	deg	cm	—	cm	—	deg
A-Ang-90	YES	90	0.1	13.2	1.2	0.9	86
A-Ang-75	YES	75	0.1	14.6	1.0	0.7	72
A-Ang-60	No	60	0.1	13.6	0.6	0.5	58
A-Ang-45	No	45	0.1	13.2	0.4	0.3	43
A-Ang-0	No	0	0.1	13.4	0.0	0.0	0
B-Ang-90	YES	90	0.1	33.2	3.2	1.0	88
B-Ang-60	(No)	60	0.1	33.3	1.6	0.5	59
B-Ang-45	No	45	0.1	33.9	1.0	0.3	44
B-Ang-0	No	0	0.1	33.6	0.0	0.0	0
A-Rad-01	YES	90	0.1	13.2	1.2	0.9	86
A-Rad-14	No	90	1.4	1.0	0.0	0.0	8
A-Rad-75	No	90	7.5	0.2	0.0	0.0	0
B-Rad-01	YES	90	0.1	33.2	3.2	1.0	88
B-Rad-14	YES	90	1.4	2.5	2.0	0.6	66
B-Rad-75	No	90	7.5	0.5	0.0	0.0	0

Table 2 lists the values of d, Γ, and Φ, for the experiments conducted. Experiments are tabulated in the same order as in Table 1, and as before, a gray background indicates that the experiment was observed to form a recirculating bulge. Examination of Table 2 shows that the separation ratio, Γ, (and likewise the impact angle, Φ) discriminate between experiments in which a recirculating bulge forms and those in which it does not. Note that in every case in which a recirculating bulge was observed to form, the value of the separation ratio was greater than 0.5. Conversely, values of the separation ratio less than 0.5 are associated with experiments that did not develop a recirculating bulge. Figure 8 shows this data graphically, with the separation distance, d, plotted on the ordinate, and the inertial radius, u/f, plotted on the abscissa. The dashed line corresponds to a separation ratio value of $\Gamma = 0.5$. Values to the right of the line have larger values of the separation ratio ($\Gamma > 0.5$); all experiments conducted in this part of the graph are observed to have formed a recirculating bulge (denoted by the circles). Values to the left of the line have smaller values of the separation ratio ($\Gamma < 0.5$) and do not form a recirculating bulge (denoted by triangles).

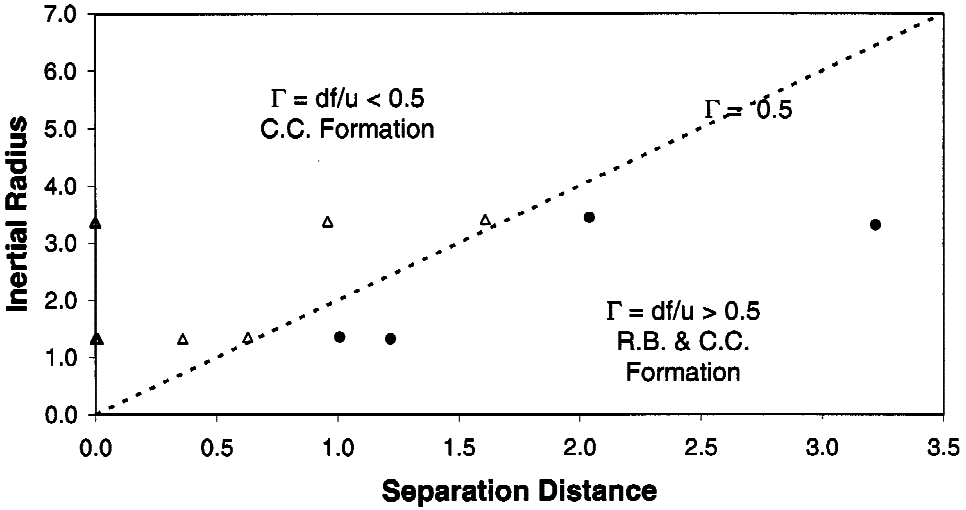

Figure 8. Graph of the predicted separation distance, d, plotted against the inertial turning radius, u/f. Values of the separation ratio, $\Gamma = df/u$, equal to 0.5 are shown as the dashed line bisecting the graph. Values of the separation ratio, $\Gamma > 0.5$, comprise experiments in which recirculating bulge formation is observed to occur. Conversely, values of the separation ratio, $\Gamma < 0.5$, are associated with experiments in which no recirculating bulge is observed. Experiments in which a recirculating bulge region formed are plotted with a solid circle and fall to the right of the dashed line ($\Gamma > 0.5$). Experiments in which a recirculating bulge did not form are plotted with an open triangle and fall to the left of the dashed line ($\Gamma < 0.5$).

c. The importance of impact angle, Φ

As shown in Eq. 7, the separation ratio, Γ, can also be expressed in terms of an impact angle, Φ. A value of 0.5 in the separation ratio ($df/u = 0.5$) corresponds to an impact angle of 60-degrees ($\Phi = 60°$). Thus, as seen in Table 2, all experiments with recirculating bulge formation occur in experiments for which the value of the impact angle, $\Phi >$ 60-degrees. Experiments with smaller values of the impact angle, θ, did not form a recirculating bulge. While the separation ratio is a useful measure of recirculating bulge formation, ultimately the physics of the formation of the recirculating bulge lies in the response of the jet to its impact with the coastal wall.

The flowfield of a baroclinic jet impinging on a vertical wall in a rotating system was examined by Whitehead (1985). The mechanism which controls recirculating bulge formation is likely to occur at this impact point, and thus we review his solution here. His solution was based on a two-layer system: a dynamic buoyant layer above a semi-infinite dense lower layer. Figure 9 is an adaption of Whitehead's Figure 2; it depicts a schematic of the flow configuration. A baroclinic jet impinging upon a wall splits into two jets, one traveling upshelf, and the other downshelf. The relative flowrates of the upshelf and downshelf jets are determined by the streamline at which the initial jet bifurcates.

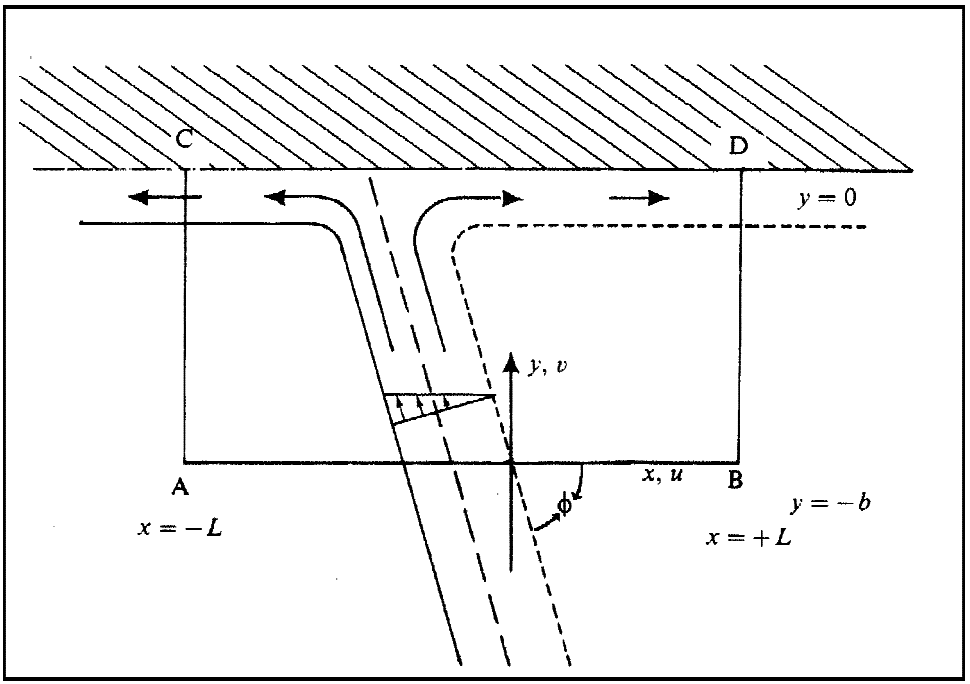

Figure 9. Schematic adapted from Whitehead (1985) depicting a buoyant jet encountering a wall in a rotating system. The schematic was altered to conform to the variable conventions used in this study. Whitehead (1985) examined the momentum and volume flux transport upstream (to the left in the schematic) and downstream (to the right) based upon the impact angle, Φ. For the arguments presented in this paper, the critical impact angle occurs just as the initial buoyant jet impacts the wall. The resulting impact forms two jets, one moving upstream, the second moving downstream. The magnitude of the impact angle, and thus the volume flux in the jets, determine whether or not recirculating bulge formation will subsequently occur.

Whitehead (1985) solves for the upshelf and downshelf volume flux starting with the depth averaged momentum equations written as:

$$hu\frac{\partial u}{\partial x} + hv\frac{\partial u}{\partial y} - fvh = -\frac{1}{2}g'\frac{\partial}{\partial x}(h^2) \tag{8}$$

$$hu\frac{\partial v}{\partial x} + hv\frac{\partial v}{\partial y} + fuh = -\frac{1}{2}g'\frac{\partial}{\partial y}(h^2). \tag{9}$$

These two equations, integrated in the control volume shown in Figure 9, and combined with continuity, result in an integrated momentum balance expressed as:

$$\int_{-b}^{0} hu^2 dy\Big|_{x=-L}^{x=+L} + \int_{-L}^{+L} huv dx\Big|_{x=-b}^{x=0} = 0. \tag{10}$$

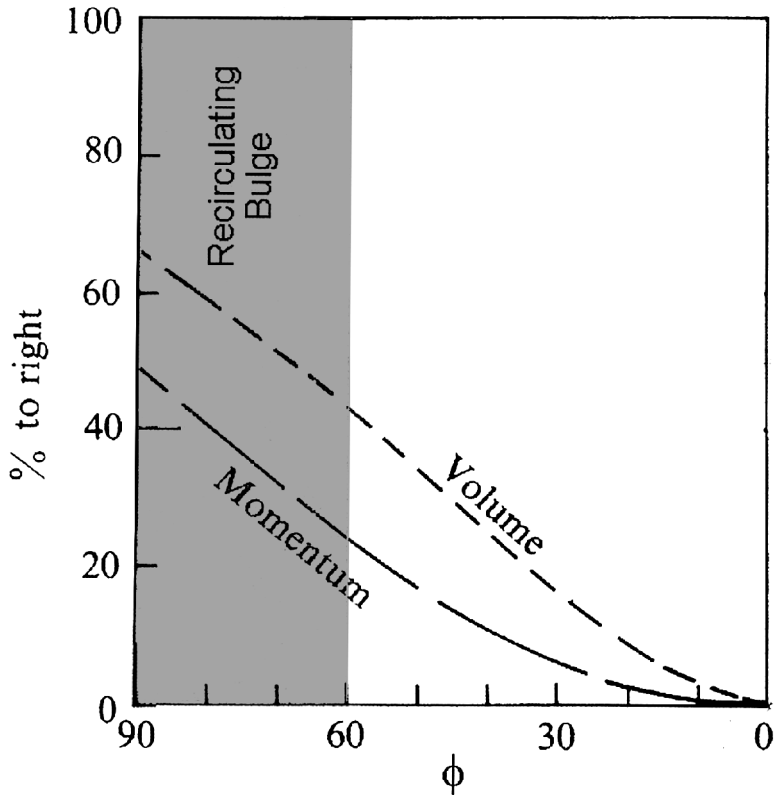

Figure 10. Graph in which the percentage momentum and volume returned to the source region is plotted as a function of impact angle, Φ. This graph was adapted from Whitehead (1985). The percentages are calculated for a zero potential vorticity baroclinic jet. The shaded area is overlayed upon the graph of Whitehead (1985) based upon the results of the study presented in this paper. The shaded region indicates impact angles for which a recirculating bulge was observed to form (angles larger than 60 degrees). This corresponds to a recirculating volume flux of approximately 50% of the source flux necessary to initiate a recirculating bulge region.

Note that the momentum balance of Eq. 10 lacks Coriolis terms; they are introduced into the problem indirectly as they determine the height and velocity profiles (h, u, and v) used to solve Eq. 10 based upon the potential vorticity of the impinging jet. Whitehead (1985) includes solutions of this system of equations for jets of semi-geostrophic profile with zero potential-vorticity. Figure 10 is a reproduction of his solution for a zero potential-vorticity jet for impact angles between 0° (parallel to the wall) and 90° (perpendicular to the wall). The percentage of volume and momentum flux flowing upshelf (returning to the source region) is shown as a function of impact angle.

For the experiments conducted in this study, the critical impact angle, Φ, is approximately 60°. For angles larger than this critical value, a recirculating bulge was observed to

form. The percentage of volume and momentum flux traveling upshelf can be seen as a function of impact angle. Figure 10 has been marked with a shaded region: values within this region correspond to impact angles larger than 60°. Figure 10 shows that an impact angle of 60° corresponds to approximately 25% of the total momentum flux and approximately 50% of the total volume flux being transported upshelf (i.e., return flow) toward the bay exit.

In examining the results of this experimental study (and others, notably Klinger, 1994b) in which recirculating bulge formation is observed to be a function of impact angle, the results of the theory of recirculating bulge formation being linked to the flow force of the downshelf coastal current (Pichevin and Nof, 1997; Nof and Pichevin, 2001) should be discussed. Their theory requires that the recirculating bulge grows offshore at a rate such that the Coriolis force of its offshore growth balances the momentum force of the downshelf coastal current. We find in our experiments that a recirculating bulge forms above a critical impact angle. The bulge growth is found to occur in a similar manner to their numerical results, although not their analytical predictions (this is discussed in the companion paper, Avicola and Huq, 2003).

d. Comparison of results

As discussed in Section 3a, our results were found to be in good agreement with the experiments of Bormans and Garrett (1989) for the dependence of the formation of a recirculating bulge with variations in exit radius of curvature. However, we found that the bay exit-angle was also a key parameter in determining the state of the resulting flow.

Klinger (1994b) also examined the role of exit-angle in recirculating bulge formation. His experiments found recirculating bulge formation would occur at angles greater than 45°, as opposed to the 60° found in these experiments. Two obvious differences between the two experiments exist. First, Klinger's (1994b) experiments used a dam-break source, while this study employed a steady pumped flow. Second, Klinger's (1994b) configuration was a flow that rounded a corner but was unconstrained on the seaward side ($K \gg 1$), while our experiment were with a flow that exited a narrow bay ($K = 1$).

Therefore, a possible explanation for this difference is a discrepancy in the vorticity profile across the current as it rounds the corner, either induced by differences in the outflow generation mechanism, or more likely, due to the outflow Kelvin number variations between the two experiments. The experiments of this paper (due to the $K = 1$ constraint) are characterized by a outflow jet with strong cyclonic and anticyclonic vorticity on the left and right side of the jet (Fig. 2) with zero-velocities on both walls. In contrast, Klinger's (1994b) experiments are most likely characterized by a weak cyclonic vorticity offshore, with a return flow (returning toward the bay) flowing back toward the dam-break source offshore of the buoyant jet. Horner, *et al.* (2000) also presented experimental observations of buoyant outflows with results in which the formation of a recirculating bulge depended upon the outflow velocity (with critical impact angles between 45° and 60°). These experiments were conducted with yet another experimental

setup, but notably, the experiments were conducted with the equivalent of a wide ($K \gg 1$) 'bay exit.'

Thus, we speculate that this may account for the differences between the observed experiments. This suggests a third parameter (which we did not examine in this study); namely, that the bay exit Kelvin number may be an important parameter in determining the fate of such flows. Furthermore, this suggests that the vorticity profiles of the impacting jet and the subsequent return flow (Fig. 9) are dynamically important.

4. Conclusions

A limitation of the results of this study should be noted. The experiments were conducted such that the fluid was released from a source of $K \sim 1$. Therefore, the experiments conducted were performed over a small range of outflow Froude numbers ($0.5 < \mathrm{Fr} < 0.75$): the dependence of recirculating bulge formation on outflow Froude numbers outside this range is not examined in this study. However, the Froude numbers range of the experiments conducted is similar to observed bay exit Froude numbers in the coastal ocean. Typical oceanic outflows range from moderately supercritical to subcritical, based upon the Kelvin number of the outflow. The Columbia River is an example of a supercritical outflow, with a narrow exit width $K \sim 0.5$ (based on a $R \sim 8$ km and a $W \sim 4$ km (Hickey *et al.,* 1998)) corresponding to a Froude number value of approximately 2. More typically, buoyant outflows tend to have subcritical outflows based on wide exit widths, such as the Delaware Bay outflow with a $K \sim 4$ (based on a $R \sim 6$ km and a $W \sim 24$ km (Münchow and Garvine, 1993a,b)), which corresponds to a Froude number value of approximately 0.25.

A second issue exists regarding the deceleration of the buoyant outflow. The geometric arguments that are used to produce Eqs. 5, 6, and 7 (and which predict the separation distance, d, the separation ratio, Γ, and the impact angle, Φ) assume that the velocity of the buoyant outflow is constant. However, experiments have shown that a buoyant outflow released parallel to the wall from a $K \sim 1$ exit (with an initial $\mathrm{Fr} \sim 1$) tends to mix and slow, transforming from a two-layer coastal current to a broader, slower, continually stratified coastal current. As the coastal current broadens and slows, it evolves to a flow with a Froude number value of approximately 0.25. Such a value has been observed in both experiments (e.g., Avicola and Huq, 2002) and oceanic flows (e.g., Garvine, 1995). Consequently, in the period during which the buoyant outflow exits the bay, separates from the wall, makes its inertial turn, and finally impacts the coastal wall downshelf, the flow may undergo some deceleration. If the outflow velocity does decrease during the inertial turn, the actual impact angle will be steeper than the predicted impact angle of Eq. 7. Observations of the experiments in this study show that if such deceleration does occur, the effect is small.

Previous studies focused on the mechanism of flow separation from a coastal wall as the mechanism responsible for generating a recirculating bulge (Whitehead, 1985; Bormans and Garrett, 1989; Klinger, 1994a). The role of the radius of curvature in flow separation

was addressed in these works. It was found that a bay exit Rossby number ($Ro = u/fr_c$), defined as the ratio of the inertial turning radius of the jet, u/f, to the sharpness of the exit corner, r_c, dictates whether or not the buoyant current would separate from the wall. However, the exit angle was assumed large. Flow separation was always found to form a recirculation region. Experiments presented in this study show that experiments possessing large values of the bay exit Rossby number ($Ro = u/fr_c = O(10–100)$) do not always form a recirculating bulge. A parameter space involving only the radius of curvature of the exit is incomplete: the bay exit angle, θ, is influential in determining whether a recirculating bulge forms. It was observed that variations in the bay exit angle, θ, produced a recirculating bulge in some cases, and no bulge in others.

This study suggests that for bulge formation to occur, not only must flow separation take place at the bay exit, but also that the flow separation must be of sufficient magnitude. It has been demonstrated that the ratio of the separation distance, d, to the radius of the internal turning radius u/f can be combined to form the dimensionless variable, $\Gamma = df/u$. This dimensionless parameter usefully discriminates whether or not a recirculating bulge region forms for experiments with variable exit angle ($0° < \theta < 90°$) and radius of curvature ($0 < r_c < \infty$). It is demonstrated that buoyant outflows with values of the separation ratio larger than 0.5 ($\Gamma = df/u > 0.5$) will produce a recirculating bulge region.

Finally, for the coastal geometric variations used in this study, the separation ratio can be expressed as an impact angle, Φ. The impact angle denotes the angle at which the buoyant fluid re-encounters the coastal wall after separation. This is an important interpretation, as the impact angle governs the dynamics of the subsequent upshelf and downshelf flows diverging from the impact point. It was shown that for impact angles larger than 60° ($\Phi > 60°$) a recirculating bulge forms. However, the mechanism which controls this critical angle has not been established in this work, and remains an open question. We speculate (as discussed in Section 3d) the vorticity distribution across the flow near the impact point is dynamically significant and suggest this is an area where further research may be fruitful.

Acknowledgments: We are appreciative of Dean Thoroughgood and the Okie fellowship for financial support. Additionally, the incisive, critical comments of A. D. Kirwan, Jr. have greatly improved this paper.

REFERENCES

Avicola, G. and P. Huq. 2002. Scaling analysis for the interaction between a buoyant coastal current and the continental shelf: experiments and observations. J. Phys. Oceanogr., *32,* 3233–3248.

——— 2003. The characteristics of the recirculating bulge region in coastal buoyant outflows. J. Mar. Res., *61,* 435–463.

Bacon, S., G. Reverdin, I. G. Rigor and H. M. Snaith. 2002. A freshwater jet on the East Greenland shelf. J. Geophys. Res., *107*(C7), 10.1029/2001JC000935.

Bormans, M. and C. Garrett. 1989. A simple criterion for gyre formation by the surface outflow from a strait, with application to the Alboran Sea. J. Geophys. Res., *84,* 3733–3742.

Bowman, M. J. and R. L. Iverson. 1978. Estuarine and plume fronts, *in* Workshop on Oceanic Fronts in Coastal Processes, Marine Sciences Research Center, Stony Brook, NY, May 25–27, Proceedings, Springer-Verlag, NY, 87–104.

Chao, S-Y. and W. C. Boicourt. 1986. Onset of estuarine plumes. J. Phys. Oceanogr., *16,* 2137–2149.

Donde Va Group. 1984. An oceanographic experiment in the Alboran Sea. EOS Trans., AGU, *65,* 682–683.

Garvine, R. W. 1995. A dynamical system for classifying buoyant coastal discharges. Cont. Shelf Res., *15,* 1585–1596.

Hickey, B. M., L. J. Pietrafesa, D. A. Jay and W. C. Boicourt. 1998. The Columbia River Plume study: subtidal variability in the velocity and salinity fields. J. Geophys. Res., *103*(C5), 10339–10368.

Horner, A. R., D. A. Fong, J. R. Koseff, T. Maxworthy and S. G. Monismith. 2000. The control of coastal current transport, 5th International Symposium on Stratified Flows, International Association of Hydraulic Research, Vancouver, Canada, 865–870.

Jiang, X. 1995. Flow separation by interfacial upwelling in the coastal ocean, M.S. thesis, University of Victoria, 64 pp.

Kawasaki, Y. and T. Sugimoto. 1984. Experimental studies on the formation and degeneration processes of the Tsugaru warm gyre, *in* Ocean Hydrodynamics of the Japan and East China Sea, T. Ichiye, ed., D. Reidel Publishing Company, 225–238.

Klinger, B. A. 1994a. Inviscid current separation from rounded capes. J. Phys. Oceanogr., *24,* 1805–1811.

——— 1994b. Baroclinic eddy generation at a sharp corner in a rotating system. J. Geophys. Res., *99*(C6), 12515–12531.

Lanoix, F. 1974. Project Alboran: hydrologic and dynamic study of the Alboran Sea (in French). Tech Rep. 66, N. Atl. Treaty Org., Brussels.

Münchow, A. and R. W. Garvine. 1993a. Buoyancy and wind forcing of a coastal current. J. Mar. Res., *51,* 293–322.

——— 1993b. Dynamical properties of a buoyancy-driven coastal current. J. Geophys. Res., *98*(C11), 20063–20077.

Nof, D. and T. Pichevin. 2001. The ballooning of outflows. J. Phys. Oceanogr., *31,* 3045–3058.

Oey, L-Y. and G. L. Mellor. 1993. Subtidal variability of estuarine outflow, plume, and coastal current: A model study. J. Phys. Oceanogr., *23,* 164–171.

Pichevin, T. and D. Nof. 1997. The momentum imbalance paradox. Tellus, *48A,* 298–319.

Whitehead, J. A. 1985. The deflection of a baroclinic jet by a wall in a rotating fluid. J. Fluid Mech., *157,* 79–93.

Yankovsky, A. E. and D. C. Chapman. 1997. A simple theory for the fate of buoyant coastal discharges. J. Phys. Oceanogr., *27,* 1386–1401.

Received: *10 March, 2003;* revised: *27 May, 2003.*